Journal of Systems Engineering and Electronics
Vol. 34, No. 5, October 2023, pp.1171 – 1181

Non-LOS target localization via millimeter-wave automotive radar

LIU Zhaoyu[1,2], ZHANG Wenli[1,2,*], ZHENG Jingyue[1], GUO Shisheng[1,*], CUI Guolong[1], KONG Lingjiang[1], and LIANG Kun[1,2]

1. School of Information and Communication Engineering, University of Electronic Science and Technology of China, Chengdu 611731, China; 2. School of Intelligent Engineering, Zhengzhou University of Aeronautics, Zhengzhou 450046, China

Abstract: This paper considers the non-line-of-sight (NLOS) vehicle localization problem by using millimeter-wave (MMW) automotive radar. Several preliminary attempts for NLOS vehicle detection are carried out and achieve good results. Firstly, an electromagnetic (EM) wave NLOS multipath propagation model for vehicle scene is established. Subsequently, with the help of available multipath echoes, a complete NLOS vehicle localization algorithm is proposed. Finally, simulation and experimental results validate the effectiveness of the established EM wave propagation model and the proposed NLOS vehicle localization algorithm.

Keywords: millimeter-wave (MMW) automotive radar, multipath propagation model, non-line-of-sight (NLOS) vehicle localization.

DOI: 10.23919/JSEE.2023.000070

1. Introduction

Recently, with the rapid development of the intelligent vehicle industry, its safety has attracted extensive attention. In order to improve the safety of pedestrians and drivers, a variety of new sensing technologies have been applied to the environmental perception of intelligent vehicles. Among them, radar is becoming one of the effective means of vehicle environmental perception with its excellent performance. At present, common automotive radar systems are utilized to improve vehicle safety by detecting or predicting the motion state of the vehicles in line-of-sight (LOS) areas [1,2]. However, in practice, there are often multiple vehicles in series. The existing technology is basically unable to predict the deceleration/braking actions of non-LOS (NLOS) vehicles [3−6]. In this case, driving safety is mainly affected by the response speed of the vehicle directly ahead to the sudden braking, deceleration, and other operations of the preceding vehicle. If the vehicle has the ability to detect both LOS vehicles and NLOS vehicles, the risk of serial collisions will be greatly reduced. In recent years, the problem of NLOS target detection based on automotive radar has gradually attracted the attention of the public.

In order to realize the effective detection of vehicles in NLOS area by automotive radar, scholars have proposed a variety of detection schemes to deal with different application scenarios. Johansson et al. [7] set the application scenario as an urban road environment, so that based on the wall reflection path of electromagnetic waves, the X-band radar system could realize the detection of NLOS moving vehicles in the corner. However, this method requires a suitable wall as a reflective surface at the road intersection, which obviously does not have a broad application prospect. Solomitckii et al. [8−10] proposed to install a reflector at the corner of the road to realize the detection of NLOS approaching vehicles at road intersections by millimeter-wave (MMW) automotive radar. Although this method can provide a stable reflection path for NLOS vehicle detection, it increases the construction cost of the road. Zhang et al. [11−13] proposed a multi-point vehicle positioning technology through MMW transmission. This technology uses the multipath reflection from the target vehicle to the sensing vehicle, so that the sensing vehicle can quickly capture the shape and position information of the NLOS target vehicle with the help of multipath reflection. This method can obtain the position of NLOS vehicle, but the signals of radar vehicle and NLOS vehicle are cooperative, and the detection method of NLOS vehicles has not been verified in the

Manuscript received March 01, 2020.
*Corresponding authors.
This work was supported by the National Natural Science Foundation of China (62201510;62001091;61801435;61871080;61801435), the Initial Scientific Research Foundation of University of Science and Technology of China (Y030202059018051), Yangtze River Scholar Program, Sichuan Science and Technology Program (2019JDJQ0014), 111 Project (B17008), Henan Provincial Department of Science and Technology Research Project (202102210315;212102210029;202102210137).

experimental data.

In addition, Aladsani et al. [14] realized the high-precision positioning of short-range NLOS pedestrians and vehicles by comprehensively using MMW radar imaging technology and mobile communication technology. Scheiner et al. [15] proposed an NLOS target detection and tracking method based on artificial neural network, and verified the effectiveness of the algorithm in the actual road environment by using vehicle Doppler radar.

From the published literature, in order to realize the detection of NLOS moving vehicles by on-board radars, the existing schemes need either to detect the presence of appropriate walls as reflectors in the scene, or to manually install reflectors and other equipment, which is obviously not conducive to the real-time detection of NLOS moving vehicles by on-board radars. Therefore, this paper proposes an NLOS target localization via MMW automotive radar, which uses the ground reflection path of electromagnetic (EM) wave as the detection path of NLOS front-front vehicle. This scheme does not need to install reflectors and is not limited by scene buildings. It can realize the rapid and stable detection of NLOS vehicles in different scenarios.

The rest of this paper is organized as follows. In Section 2, the front-front vehicle signal propagation model is presented. Then, the signal processing method, which includes signal pretreatment, target detection, and target localization is presented in Section 3. In Section 4, the EM simulation and experimental data are used to validate the effectiveness of the proposed signal propagation model and the signal processing algorithm. Section 5 summarizes this paper.

2. Signal model

2.1 Signal model construction

Consider an NLOS front-front vehicle detection scenario, consisting of MMW automotive radar, front vehicle and front-front vehicle, as shown in Fig. 1(a). It is clearly seen that the front vehicle is in LOS area of the radar, and there is a direct propagation path from the radar to the front vehicle. While the front-front vehicle is located at the NLOS area of the radar, so there is no direct propagation path from the radar to the front-front vehicle. However, it is found that in the presence of specular reflection, the echo signal of the reflection path can be utilized to detect the hidden front-front vehicle. That is to say, the multipath propagation of EM wave can be used to realize the detection of front-front vehicle.

In this paper, for ease of understanding, we define these two paths as Path 1 and Path 2. Specifically, for Path 1, which can be regarded as an LOS path, the EM wave propagates along the path O–B–O, and the front vehicle can be detected by Path 1. In addition, we also explore the EM wave propagate along the path O–A–P–A–O (Path 2), which can be exploited to detect the front-front vehicle, as shown in Fig. 1(b).

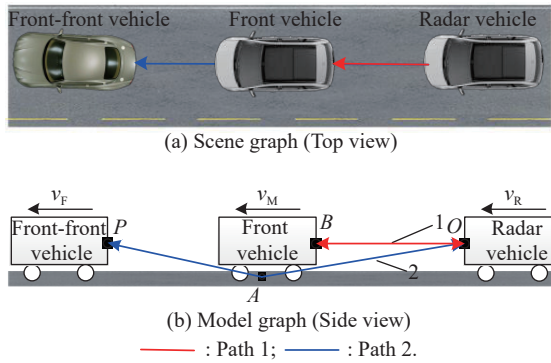

Fig. 1 Schematic diagram of NLOS signal propagation model

Assume that the centroids of the three vehicles are on the same straight line, and a single input multiple output (SIMO) MMW radar system is employed. Specifically, "O" is marked as the origin position, Q receivers R_1, $R_2,\cdots,R_Q$ are placed along a line with the interelement spacing $\lambda/2$, where λ denotes the wavelength and v_F, v_M, v_R represent the motion speeds of the radar vehicle, the front vehicle and the front-front vehicle respectively. The coordinates of the qth receiver is denoted as (x_{R_q}, y_{R_q}).

Let $s(t)$ denote the linear frequency modulated continuous wave transmitted signal, which has a form as

$$s_n(t) = A_0 \exp(\mathrm{j}2\pi f_0 t + \mathrm{j}\mu t^2)u(t) \tag{1}$$

where $n\,(n = 1, 2, \cdots, N)$ denotes the nth period, A_0 denotes the signal amplitude, f_0 represents the carrier frequency, $\mu = B/T$ is the frequency modulation rate, while B denotes the signal bandwidth, and T is the sweep time of each period, $u(t)$ denotes the rectangle function and can be expressed as

$$u(t) = \begin{cases} 1, & (n-1)T < t < nT \\ 0, & \text{others} \end{cases}. \tag{2}$$

Based on the above propagation model of EM wave, the received echo signal $y(t)$ can be denoted by

$$y(t) = \sigma_1 s(t-\tau_1)\mathrm{e}^{\mathrm{j}\varphi_1} + \sigma_2 s(t-\tau_2)\mathrm{e}^{\mathrm{j}\varphi_2} + \xi(t) \tag{3}$$

where σ_1 and σ_2 represents the reflection coefficient of the front vehicle and the front-front vehicle respectively. φ_1 and φ_2 denote the domain phase shift of the front vehicle and the front-front vehicle respectively. $\xi(t)$ is the superposition of the background noise and the environment interference. τ_1 and τ_2 is the time delay related to the propagation path p_1 and p_2. The calculation equa-

tions of τ_1 and τ_2 are described as

$$\begin{cases} \tau_1 = \dfrac{p_1}{\mathrm{c}} \\ \tau_2 = \dfrac{p_2}{\mathrm{c}} \end{cases} \tag{4}$$

where c represents the speed of light.

2.2 Influencing factors of the system

In practical application, the height from the ground and the horizontal inclination of the antenna directly affect the strength of the NLOS echo signal, and then affect the detection performance of the NLOS target. Therefore, Wavefarer software is used to analyze the optimal height from the ground and horizontal inclination of the antenna respectively.

The experimental scenario is shown in Fig. 2. Herein, the carrier frequency of the radar is 77 GHz, the initial coordinate of the MMW radar is located at (0 m, 0 m), the initial distance between the front vehicle and the MMW radar is 10 m, and the initial distance between the front vehicle and the front-front vehicle is 5 m. The velocity of the MMW radar vehicle and the front-front vehicle is 3 m/s, and the front vehicle is stationary. The initial heights of the MMW radar, the front vehicle, and the front-front vehicle are all 0.35 m, and the initial inclination angle of the MMW radar is 0°. Analyze the influence of antenna horizontal inclination and radar placement height on the front-front vehicle.

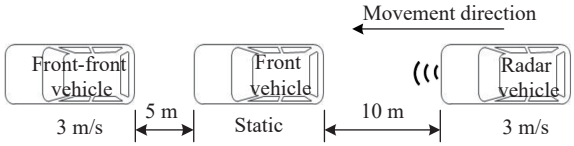

Fig. 2 Simulation diagram of NLOS front vehicle detection

(i) Case 1: Different horizontal angles of the antenna

Under the original parameters, the horizontal inclination of the antenna is set to 0°, 5°, 10°, and 15°, respectively, and the range profiles of the echo data in the corresponding inclination frame is obtained as shown in Fig. 3.

It can be seen from Fig. 3 that with the increase of the horizontal inclination angle of the antenna, the echo energy of the preceding vehicle shows a trend of increasing first and then weakening, and the optimal horizontal inclination angle of the antenna is 5°.

(ii) Case 2: Different placement heights of radar

Set the horizontal inclination of the antenna to 5°, and adjust the radar heights to 0.15 m, 0.25 m, and 0.35 m, respectively. The range profiles of the echo data in the frame is obtained as shown in Fig. 4.

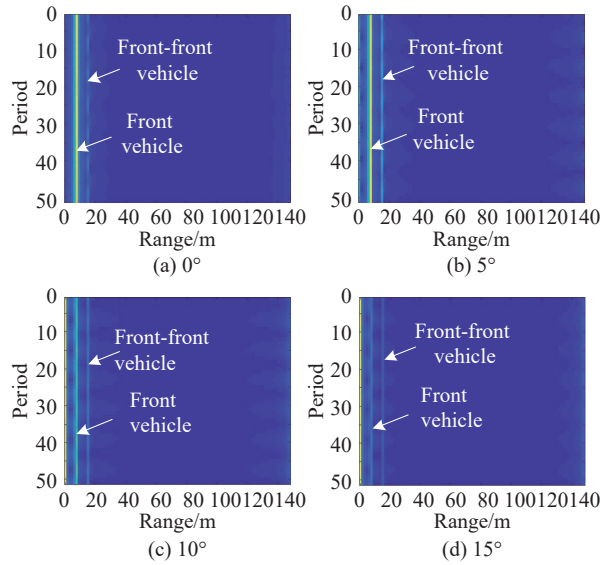

Fig. 3 Range profiles of the different antenna horizontal inclination

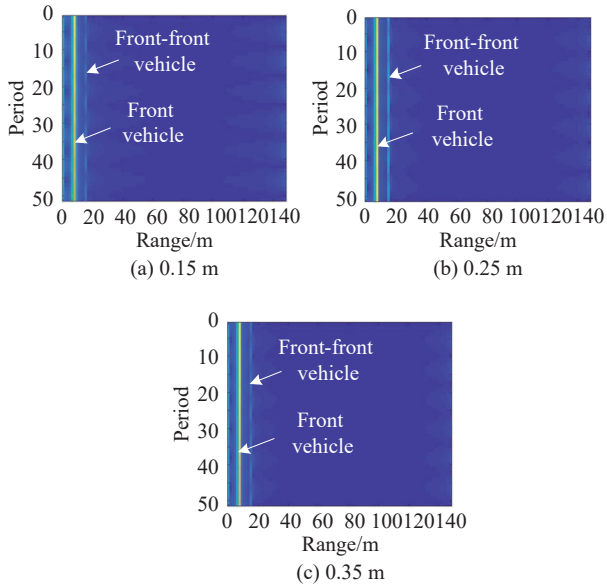

Fig. 4 Range profiles of the different placement heights of radar

It can be seen from Fig. 4 that as the height of the radar from the ground increases, the echo energy of the front-front vehicle also shows a trend of increasing first and then decreasing, and the optimal height of the antenna from the ground is 0.25 m.

Based on the above Wavefarer simulation results, it can be seen that the placement position of the MMW radar directly affects the strength of the echo signal of the front-front vehicle. Only by adjusting the height from the ground of the radar and the horizontal inclination of the antenna according to the application scenario of the system, can the effective detection of the front-front vehicle be realized.

3. The proposed algorithm

In this section, we propose a signal processing method for front-front vehicle detection by exploiting MMW automotive radar. And the signal processing method contains three steps: signal pretreatment, target detection, target localization.

3.1 Signal pretreatment

Assume that the original echo signal $\boldsymbol{Y}_{\mathrm{E}q}$ for the qth $(q=1,2,\cdots,Q)$ receiver is expressed as

$$\boldsymbol{Y}_{\mathrm{E}q}=[\boldsymbol{Y}_1,\boldsymbol{Y}_2,\cdots,\boldsymbol{Y}_i,\cdots,\boldsymbol{Y}_M]\in\mathbf{C}^{M\times N} \tag{5}$$

where $\boldsymbol{Y}_i\in\mathbf{C}^{1\times N}$ is the ith echo signal, M is the number of echo samples, and N is the number of sampling points of echo signal.

In the front-front vehicle detection system, both the radar system and the front-front vehicle are in motion state. Therefore, in order to reduce the difficulty of echo signal processing, we divide the original echo signals into groups by period T, which is less than the range resolution of the radar. Under this condition, the radar system in period T is approximately stationary. According to the above grouping method, the grouping results of the echo signals are as follows:

$$\boldsymbol{Y}'_{\mathrm{E}q}=[\boldsymbol{Y}'_1,\boldsymbol{Y}'_2,\cdots,\boldsymbol{Y}'_k,\cdots,\boldsymbol{Y}'_P]\in\mathbf{C}^{P\times N} \tag{6}$$

where $\boldsymbol{Y}'_k\in\mathbf{C}^{T\times N}$ is the new kth echo signal, and $P=M/T$ is the number of groups of echo signal.

Based on the echo signals after grouping, the target range profile can be obtained through fast Fourier transform (FFT). For the pth group of echo signal, the corresponding range profile can be expressed as

$$\boldsymbol{X}_p=[\boldsymbol{x}_1,\boldsymbol{x}_2,\cdots,\boldsymbol{x}_k,\cdots,\boldsymbol{x}_T]\in\mathbf{C}^{T\times N} \tag{7}$$

where $\boldsymbol{x}_k\in\mathbf{C}^{1\times N}$ is the target range profile of the kth echo signal in group p.

To remove the influence of the front vehicle and the environmental interference existed in (3), singular value decomposition (SVD) is employed [16,17]. The SVD process of the pth group of range profile is expressed as

$$\begin{cases}\boldsymbol{X}_p=\boldsymbol{U}\boldsymbol{\Sigma}\boldsymbol{V}^{\mathrm{H}}\\ \boldsymbol{\Sigma}=\mathrm{diag}(\alpha_1,\alpha_2,\cdots,\alpha_r,0,0,\cdots,0)\end{cases} \tag{8}$$

where $\boldsymbol{U}$ is a unitary matrix of order $T\times T$, $\boldsymbol{\Sigma}$ is a diagonal matrix of order $T\times N$, and $\boldsymbol{V}$ is a unitary matrix of order $N\times N$. α is the singular value of $\boldsymbol{X}_p$, and the value of α reflects the energy intensity of each sub-signal in signal $\boldsymbol{X}_p$. At this time, the range profiles of the front-front vehicle $\boldsymbol{X}_{p,\,\mathrm{Front\,-\,front}}$ can be obtained according to the magnitude of the singular value α.

Generally speaking, the range profile of the front vehicle is the feature subspace corresponding to the largest singular value α_1, and the range profile of the front-front vehicle is the feature subspace corresponding to the remaining singular values. Therefore, the range profile of the front vehicle is

$$\boldsymbol{X}_{p,\,\mathrm{Front}}=\boldsymbol{U}\alpha_1\boldsymbol{V}^{\mathrm{H}}. \tag{9}$$

And the range profile of the front-front vehicle is

$$\boldsymbol{X}_{p,\,\mathrm{Front\,-\,front}}=\boldsymbol{X}_p-\boldsymbol{U}\alpha_1\boldsymbol{V}^{\mathrm{H}}. \tag{10}$$

Therefore, by performing SVD processing on the original range profile, the range profile of the front vehicle $\boldsymbol{X}_{p,\,\mathrm{Front}}$ and the front-front vehicle $\boldsymbol{X}_{p,\,\mathrm{Front\,-\,front}}$ can be obtained respectively.

Note that the range profile after SVD has problems with spectrum expansion and noise interference. Therefore, the Gaussian Laplace (LoG) method [18,19] is used to denoising and sharpening the range profile of the front vehicle and the front-front vehicle. Define the LoG function as

$$\nabla^2G(x,y)=-\frac{1}{\pi\vartheta^4}\left(1-\frac{x^2+y^2}{\vartheta^2}\right)\cdot\exp\left(\frac{x^2+y^2}{2\vartheta^2}\right) \tag{11}$$

where x,y are the horizontal and vertical coordinates of matrix $\boldsymbol{X}_{p,\,\mathrm{Front\,-\,front}}$, and ϑ is the Gaussian standard deviation. The LoG process of $\boldsymbol{X}_{p,\,\mathrm{Front\,-\,front}}$ is expressed as

$$\begin{aligned}\boldsymbol{Z}_{p,\mathrm{Front\,-\,front}}=&\nabla^2G\cdot\mathrm{Re}(\boldsymbol{X}_{p,\mathrm{Front\,-\,front}})+\\&\mathrm{j}\nabla^2G\cdot\mathrm{Im}(\boldsymbol{X}_{p,\mathrm{Front\,-\,front}})\end{aligned} \tag{12}$$

where $\mathrm{Re}(\cdot)$ and $\mathrm{Im}(\cdot)$ represent the real and imaginary parts of $\boldsymbol{X}_{p,\,\mathrm{Front\,-\,front}}$, respectively.

Otherwise, based on the range profiles after LoG, the front-front vehicle Doppler profile can be obtained through moving targets detection (MTD) [20,21]. In other words, FFT is performed on each column of matrix $\boldsymbol{Z}_{p,\mathrm{Front\,-\,front}}$ to get the front-front vehicle Doppler profile. In this way, the front-front vehicle Doppler profile of the pth group of echo signal is expressed as

$$\boldsymbol{H}_{p,\mathrm{Front\,-\,front}}=[\boldsymbol{h}_1,\boldsymbol{h}_2,\cdots,\boldsymbol{h}_k,\cdots,\boldsymbol{h}_T]\in\mathbf{C}^{T\times N} \tag{13}$$

where $\boldsymbol{h}_k\in\mathbf{C}^{1\times N}$ is the front-front vehicle Doppler profile of the kth echo signal in group p.

3.2 Target detection

In order to achieve the accuracy of front-front vehicle range, we accumulate the front-front vehicle range profile of every T period by using the noncoherent integration method. And the calculation formula of $\boldsymbol{Z}_{p,\mathrm{Front\,-\,front}}$ is expressed as

$$\boldsymbol{F}_{p,\mathrm{Front\,-\,front}}=\sum_{k=1}^{T}\left|\boldsymbol{Z}_{p,\mathrm{Front\,-\,front}}[k]\right|\in\mathbf{C}^{1\times N}. \tag{14}$$

For the accumulated front-front vehicle range profile, the cell-averaging constant false alarm rate (CA-CFAR) is used to obtain the target range [22,23]. And the CA-

CFAR detection threshold of the pth group front-front vehicle range can be calculated by the following equation:

$$\mathrm{TH}_{\upsilon} = \left((P_{\mathrm{fa}})^{-1/n} - 1\right) \sum_{k=1}^{n} f_{p,\mathrm{Front\text{-}front}}(k) \tag{15}$$

where P_{fa} is the constant false alarm probability, and n denotes the number of the reference range cells around the tested cell $f_{p,\mathrm{Front\text{-}front}}$.

Herein, the judge process for the kth cell with respect to the pth accumulated front-front vehicle range profile is expressed as

$$f_{p,\mathrm{Front\text{-}front}}(k) = \begin{cases} 1, & f_{p,\mathrm{Front\text{-}front}}(k) > \mathrm{TH}_k \\ 0, & \text{others} \end{cases}. \tag{16}$$

Repeat the processing for the whole range cells, the front-front vehicle range peaks of the pth group of accumulated front-front vehicle range profile. And the front-front vehicle range l corresponds to the position information of the measured peak.

3.3 Target localization

Although the aforementioned processing can obtain the range information of the front-front vehicle, it still cannot realize the front-front vehicle localization due to the lack of the target's azimuth information. Therefore, the multi-channel phase comparison method is used to determine the target's azimuth [24–26]. And the phase comparison method exploits the phase difference between any two different channels to achieve the target's azimuth information, so the MMW radar system requires at least two antennas.

Taking the case of R_m and R_{m+1} as an example, and the schematic diagram of the phase comparison method is shown in Fig. 5.

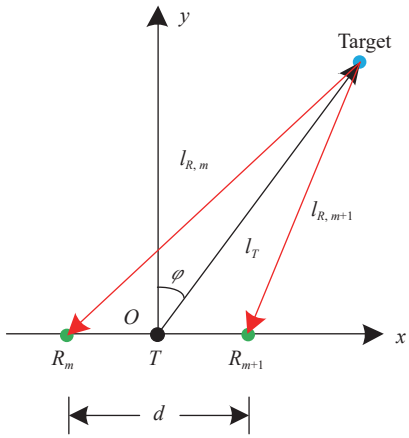

Fig. 5 Schematic diagram of phase comparison method

Assume that the propagation paths of the echo signals to the two antennas are $l_{R,m}$ and $l_{R,m+1}$. Then the phase difference between these two antennas can be calculated as

$$\phi = \frac{2\pi}{\lambda}(l_{R,m+1} - l_{R,m}) = \frac{2\pi}{\lambda} d \sin\varphi \tag{17}$$

where φ is the azimuth angle of the NLOS target, and d is the spacing of these two antennas.

It can be found by (17) that the core of the front-front vehicle azimuth solution is to obtain the phase information of the front-front vehicle corresponding to these two antennas. Based on the Doppler profile $\boldsymbol{H}_{p,\mathrm{Front\text{-}front}} \in \mathbf{C}^{T\times N}$ and the ranges l, we can obtain the phase information ψ of the front-front vehicle at range l. Then, for any two adjacent antennas R_m and R_w, the phase difference can be calculated as

$$\phi_{w,m} = \psi_w - \psi_m = \frac{2\pi}{\mathrm{c}}(l_{R,w} - l_{R,m}) f_0 \tag{18}$$

where f_0 is the carrier frequency of MMW radar.

By this time, according to (18), the front-front vehicle azimuth angle φ is given by

$$\varphi = \arcsin\left(\frac{\lambda\phi_{w,m}}{2\pi d}\right). \tag{19}$$

Combine the range l from section B and the azimuth angle φ, and the coordinates of the front-front vehicle can be calculated as

$$\begin{cases} c_x = l \cdot \sin\varphi \\ c_y = l \cdot \cos\varphi \end{cases}. \tag{20}$$

In practice, after these phase differences between different receivers, the mean value $(\bar{c}_x, \bar{c}_y)$ is calculated to improve the front-front vehicle coordinates estimation accuracy.

However, due to the moving characteristics of the radar and the front-front vehicle, the measured localization coordinate of a certain target may consist of a bunch of scattered points. Though all of these scattered points can reflect the position of the certain target, its complex distribution also affects the description of the micro motion of the target. Hence, in order to improve the detection accuracy of the front-front vehicle position, density-based spatial clustering of applications with noise (DBSCAN) method is used to analyze the localization scattered points [27–29]. And the cluster coordinate $(\hat{c}_x, \hat{c}_y)$ is the final localization of the front-front vehicle in each group.

Finally, repeating the detection and localization processing for the whole range cells, the front vehicle and the front-front vehicle coordinates of the P groups can be obtained. In addition, according to the above data analysis processing, every T period of echo signals is processed to achieve the instantaneous localizations of the front-front vehicle. The detailed operations of the proposed algorithm is shown in Algorithm 1.

Algorithm 1: Front-front vehicle detection and localization algorithm

Input: $\boldsymbol{Y}_{\mathrm{E}}$;
Output: $(\hat{x},\hat{y})$;
for $q=1,2,\cdots,Q$ **do**
Obtain $\boldsymbol{Y}'_{\mathrm{E}q}$ based on (6);
end
for $p=1,2,\cdots,P$ **do**
for $q=1,2,\cdots,Q$ **do**
Obtain $\boldsymbol{X}_{q,p}$ based on (7);
Obtain $\boldsymbol{X}_{q,p\text{ - Front}}$ and $\boldsymbol{X}_{q,p\text{ - Front - front}}$ based on (9) and (10);
Compute $\boldsymbol{Z}_{q,p\text{ - Front - front}}$ and $\boldsymbol{F}_{q,p\text{ - Front - front}}$ based on (12) and (14);
Obtain l and ψ based on (15) and (16);
end
for $w=1:Q$ **do**
for $m=1:Q$ and $w\neq m$ **do**
Compute $\phi_{w,m}$ based on (18);
end
end
Compute φ and (c_x,c_y) based on (19) and (20);
Obtain $(\hat{c}_x,\ \hat{c}_y)$ by using DBSCAN.
end

4. Simulation and experimental results

In this section, several simulation results and experimental results are provided to validate the algorithm of the front-front vehicle detection and localization.

4.1 Simulation results

To demonstrate the EM propagation process of the MMW automotive radar to front-front vehicle, and verify the correctness of the signal propagation model established in Section 2, the Wavefarer software [30] is used for simulation experiments. The simulation scenario of the front-front vehicle signal propagation model is shown in Fig. 6.

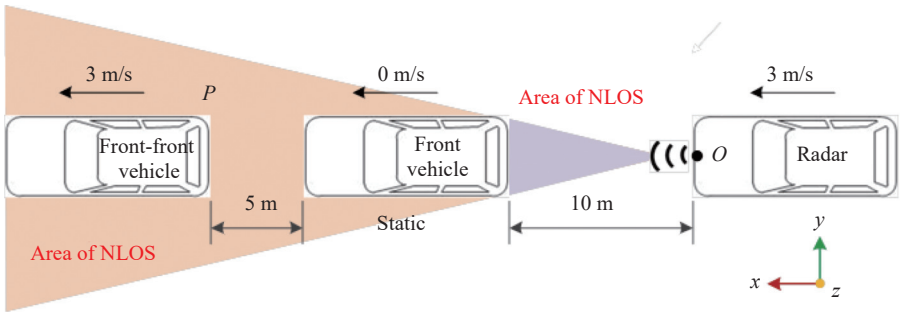

Fig. 6 Simulation model based on Wavefarer software

In this simulation experiment, the carrier frequency of the MMW radar is 79 GHz, the bandwidth is 4 GHz, the frequency modulates period is 80 μs and the sampling interval is 10 ns. The initial coordinate of the MMW radar is located at (0 m,0 m). Both the velocity of the MMW radar and the front-front vehicle are 3 m/s, and the front vehicle is stationary. The initial distance from the front vehicle to the MMW radar and the front-front vehicle are 10 m and 5 m, respectively. In addition, the heights of the MMW radar, the front vehicle, and the front-front vehicle are 0.25 m, and the horizontal inclination angle of the MMW radar is 5°.

The simulation results are shown in Fig. 7. In Fig. 7(a), we give the range profile of the simulation data. It is clear that there are two different trajectories: the left one is more obvious and closer to the radar, while the other one is shallower and slightly farther from the radar. This is mainly because the left trajectory is the direct reflection path (Path 1) of the front vehicle, and the right trajectory is the bottom reflection path (Path 2) of the front-front vehicle. In addition, the Doppler profile of the simulation data is shown in Fig. 7(b). Note that the relative velocity of the front vehicle is −3 m/s, and the relative velocity of the front-front vehicle is 0 m/s, which is consistent with the setting parameters of the simulation scenario.

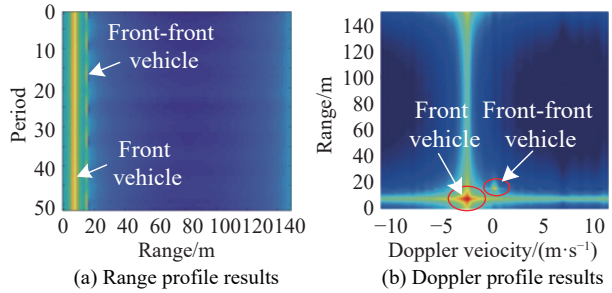

(a) Range profile results (b) Doppler profile results

Fig. 7 Simulation results of the moving vehicle

Therefore, the simulation results (shown in Fig. 8) preliminarily verify the correctness of the signal propagation model in Section 2. Then the feasibility of this signal propagation model in front-front vehicle detection will be verified by experiments.

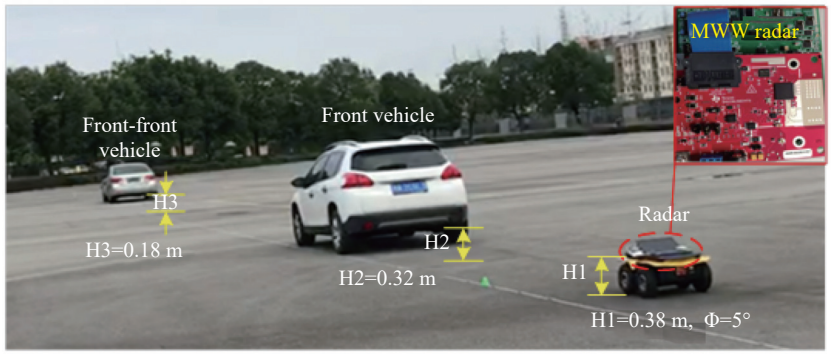

Fig. 8 Photo of MMW automotive radar NLOS front-front vehicle detection experimental scenario

4.2 Experimental results

To further validate the NLOS signal propagation model and the proposed algorithm, we perform several experiments by using the AWR1642 MMW radar with one transmitting antennas and four receiving antennas. The detailed parameters of the MMW radar are listed in Table 1.

Table 1 Parameters of MMW radar

Parameter	Value
Carrier frequency f_0/GHz	77
Bandwidth B/MHz	505
Inter-element spacing of receiving antenna d/mm	1.95
Sampling frequency/MHz	5
Pulse repetition time/μs	156
Frequency modulation slope/(MHz·μs^{-1})	9.366
Sampling points	256
Range cell/m	0.314

The experimental scenario is shown in Fig. 8. Herein, the height of the MMW radar system (H1) is 0.38 m, the horizontal inclination angle of the MMW radar is 5°. The height of the front vehicle chassis (H2) is 0.32 m, the height of the front-front vehicle chassis (H3) is 0.18 m. In the following, two experiments are carried out according to the movement of the vehicles.

(i) Case 1: Three vehicles move regularly

In the first experiment, to test the validity of the signal propagation model and the proposed algorithm. We set the initial coordinate of the MMW radar is located at (0 m,0 m), the initial distance between the front vehicle and the MMW radar is 15 m, and the initial distance between the front vehicle and the front-front vehicle is 20 m. During the experiment, the front vehicle remains the stationary state, the MMW radar moves back and forth within 3−15 m from (0 m,0 m), and the front-front vehicle moves back and forth within 20−45 m from (0 m, 0 m). Then there are 19200 periods of echo signals collected.

The range profile of channel-2 with respect to all periods of echo signals is shown in Fig. 9(a). It is can be seen that there are two different trajectories, and the range trajectory of the front vehicle is stronger than the front-front vehicle. As a result, part of the range profile of the front-front vehicle have not been revealed. Therefore, we give the range profile of the 100th group of data (shown in Fig. 9(b)). It is clearly found that, although the LOS echoes (front vehicle) have strong energy, the NLOS echoes (front-front vehicle) also have good energy distribution.

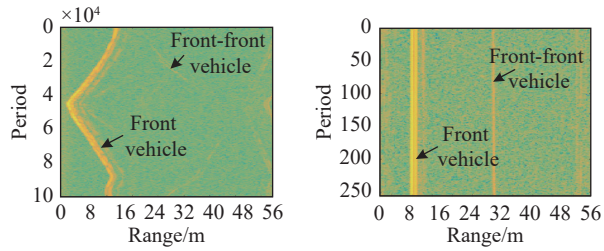

(a) The complete experimental data (b) The 100th group of data

Fig. 9 Range profiles for the first experiment

The range profiles of the front vehicle and the front-front vehicle separated by SVD are shown in Fig. 10. It can be found that the SVD algorithm can separate the range profile of the front vehicle (shown in Fig. 10(a)) and the front-front vehicle (shown in Fig. 10(b)), but the separated results have serious environment noise and interference information, such as the residual range profiles of the front vehicle in the front-front vehicle (shown in Fig. 10(b)). Otherwise, the separated target curves have serious edge blur. Therefore, LoG algorithm was used in denoising and sharpening the above range profiles, and

the denoising and sharpening results of the 100th group of data are shown in Fig. 11.

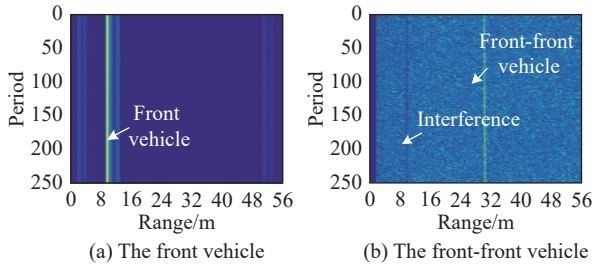

Fig. 10 Range profiles of the 100th data

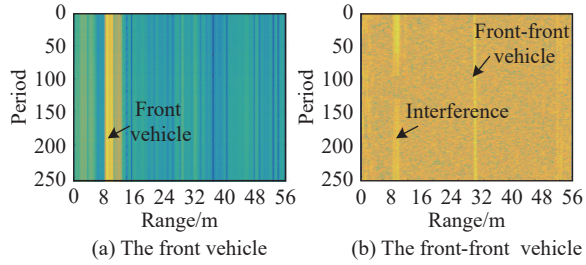

Fig. 11 Denoising-sharpening results of the 100th group of data

In Fig. 11, note that the LoG processing not only effectively suppresses the background noise in the original range profile (shown in Fig. 10), but also enhances the trajectory of the front vehicle and the front-front vehicle (shown in Fig. 11).

Then, CA-CFAR was used to detect the front vehicle and the front-front vehicle, respectively. In actual experiment, the CA-CFAR parameters like protection unit, reference unit and false alarm rate adjustment parameter of the front vehicle are 20, 35, and 3.2. And the relevant parameters of the front-front vehicle are 5, 8, and 1.8. The detection results of the 100th group of data by the above parameters are shown in Fig. 12.

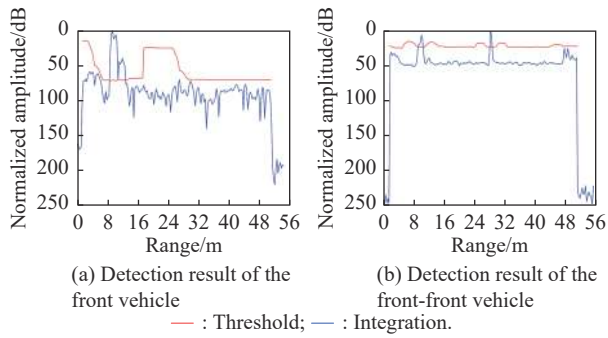

Fig. 12 CA-CFAR detection results of the 100th group of data

In Fig. 12(a), it is clear that by setting appropriate CA-CFAR parameters, the detection of the front vehicle can be effectively realized (shown in Fig. 12(a)). However, due to the influence of the residual information of the front vehicle (interference shown in Fig. 11(b)), the detection result of the front-front vehicle may be containing some information of the front vehicle (shown in Fig. 12(b)). At this time, the detection results of the front vehicle can be used as a priori information to correct the detection results of the front-front vehicle, so as to obtain an accurate detection results of the front-front vehicle.

In the following data processing, the multi-channel phase comparison method is used to determine the target's azimuth, the DBSCAN is used to analyze the localization scattered points. And the target positioning results of the 90th, 100th, and 110th groups of data are shown in Fig. 13.

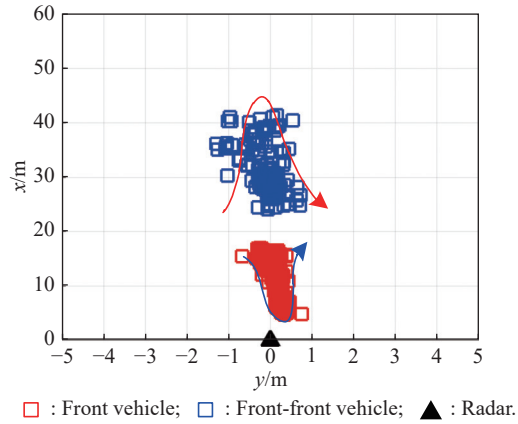

Fig. 13 Positioning results of the 90th, 100th, and 110th group of data

In Fig. 13, it can be seen that the localizations of the front vehicle and front-front vehicle are clearly presented. The measured mean relatively velocity of the front vehicle and the front-front vehicle is 3.1 m/s and 3.9375 m/s, respectively. Otherwise, the front vehicle is moving close to the MMW radar, while the front-front vehicle is moving far away from the MMW radar in these time from 90th to 110th, which is consistent with the actual trajectory of the front and the front-front vehicle.

In Fig. 14, we give the positioning results of all experimental data. Herein, the track of the front vehicle is shown by the blue line, and the track of the front-front vehicle is shown by the red line. From the moving curve, note that the localization range of the front vehicle is 3.21−17.66 m, the localization range of the front-front vehicle is 21.87−41.74 m. In addition, affected by the residual signal of the front vehicle, a few positioning results of the front-front vehicle appear in the positioning area of the front vehicle. Fortunately, most of the front vehicle and the front-front vehicle positions are relatively accurate.

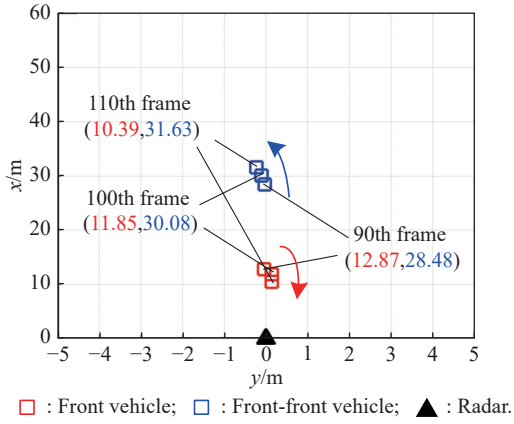

Fig. 14 Positioning results of the first complete experimental data

(ii) Case 2: Three vehicles move irregularly

In the second experiment, to test the universality of the signal propagation model and the proposed algorithm, it is also set that the initial coordinate of the MMW radar system is located at (0 m, 0 m), the initial distance between the front vehicle and the MMW radar is 15 m, and the initial distance between the front vehicle and the front-front vehicle is 20 m. Different from the first experiment, during the experiment, all of the MMW radar system, the front vehicle and the front-front vehicle move irregularly.

Similarly, the range profile of channel-2 with respect to all periods of echo signals are shown in Fig. 15(a). Note that the range trajectory of the front vehicle and the front-front vehicle can be seen clearly. However, there are many weak interference signals on the right side of the range profile plane. In order to clearly display the range profile of the front vehicle, the front-front vehicle and the interference, we give the range profile of the 100th group of echo signal as shown in Fig. 15(b). It is clear that both the front vehicle and the front-front vehicle have strong energy distribution. However, the energy distribution of the interference is also relatively strong, which directly affects the positioning accuracy of the front vehicle and the front-front vehicle.

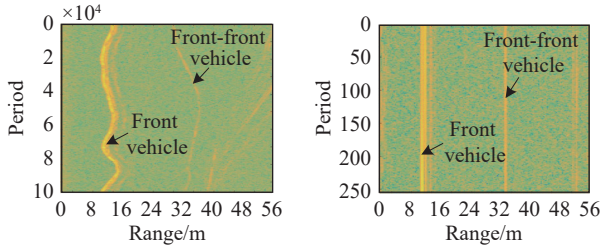

(a) The complete experimental data (b) The 100th group of data

Fig. 15 Range profiles for the second experiment

Based on the proposed signal processing algorithm in Section 3, the front vehicle and the front-front vehicle position results of the 90th, 100th, and 110th groups of data are shown in Fig.16. Note that the localizations of the front vehicle and the front-front vehicle are also clearly presented. And the measured relatively velocity of the front vehicle for the 90th and 100th group is 1.1 m/s, for the 100th and 110th group is −0.25 m/s. The measured relatively velocity of the front-front vehicle for the 90th and 100th group is 0.295 m/s, for the 100th and 110th group is 0.15 m/s. It is explained that the front vehicle moves back and forth relatively frequently, while the movement of the front-front vehicle is relatively stable.

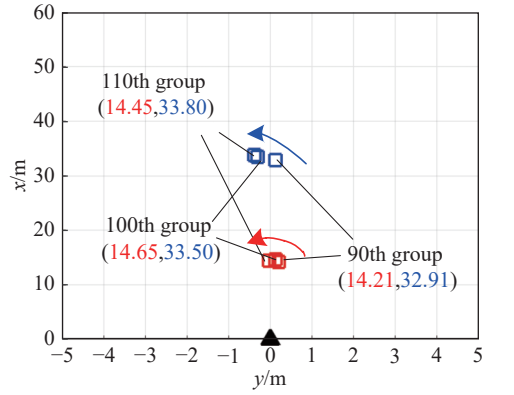

Fig. 16 Positioning results of the 90th, 100th, and 110th group of data

In Fig. 17, we also give the positioning results of the whole experimental data, and the track of the front vehicle is shown by the blue line, the localization range of the front vehicle is 11.40−18.42 m. The track of the front-front vehicle is shown by the red line, and the localization range of the front-front vehicle is 28.21−37.96 m. In addition, affected by the residual information and interference, a few positioning results of the front vehicle and the front-front vehicle is error, but most of the front vehicle and the front-front vehicle positions are relatively accurate.

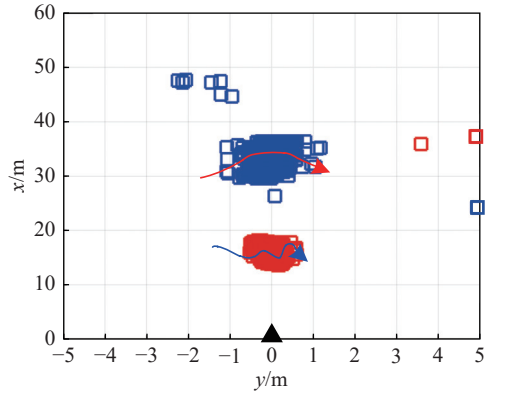

Fig. 17 Positioning results of the second complete experimental data

Analyze the experimental results of Case 1 and Case 2, it is can be seen that: (i) Both of the experiments have achieved effective detection of the front vehicle (LOS target) and the front-front vehicle (NLOS target), and the detection targets trajectory are basically consistent with the set path, which verifies the correctness of the signal propagation model; (ii) No matter how the motion state changes of the targets are measured (regular, irregular, fast, slow, etc.), the system can accurately realize the detection and localization of the targets, which verifies the effectiveness of the data processing algorithm; (iii) In this paper, the MMW automotive radar front-front vehicle detection system is built, and the effective detection range of the MMW radar system exceeds 40 m, the range resolution reaches 0.314 m, this shows the potential practical prospects of the system.

5. Conclusions

This paper constructs an NLOS signal propagation model based on MMW automotive radar, and proposes a front-front vehicle localization method with SIMO MMW radar. Based on the multipath propagation of EM wave, all of the vehicles located on the LOS and NLOS area of the radar can be detected. In summary, first of all, the echo signals are grouped by period T, and the range profiles are obtained by FFT. The SVD method is used to separate the front vehicle and the front-front vehicle, and the LoG method is used to denoise and sharpen the range profiles of the targets. Secondly, by the noncoherent-integration method, the accumulated range profiles are constructed, and the CA-CFAR technique is used to extract the range of the front vehicle or front-front vehicle. Thirdly, MTD is used to obtain the phase information of the vehicle, and according to the multi-channel phase comparison method, the azimuthal angle of the vehicle is calculated. Forthly, the DBSCAN method is used to determine the target accuracy position coordinates. Finally, several simulation and experimental results validate the correctness of the signal propagation model and the effectiveness of the proposed signal processing algorithm.

References

[1] XU Z H, BAKER C J, POONI S. Range and Doppler cell migration in wideband automotive radar. IEEE Trans. on Vehicular Technology, 2019, 68(6): 5527–5536.

[2] CHU P, ZHANG A, WANG X X, et al. Interference characterization and power optimization for automotive radar with directional antenna. IEEE Trans. on Vehicular Technology, 2020, 69(4): 3703–3716.

[3] JO K C, LEE M, KIM J S, et al. Tracking and behavior reasoning of moving vehicles based on roadway geometry constraints. IEEE Trans. on Intelligent Transportation Systems, 2017, 18(2): 460–476.

[4] SONG W J, YANG Y, FU M Y, et al. Real-time obstacles detection and status classification for collision warning in a vehicle active safety system. IEEE Trans. on Intelligent Transportation Systems, 2018, 19(3): 758–773.

[5] CHEN Y S, CHIU S C, HSIAU S S. Safe technology with a novel rear collision avoidance system of vehicles. International Journal Automotive Technology, 2019, 20(4): 693–699.

[6] SUN S Q, PETROPULU A, POOR H. MIMO radar for advanced driver assistance systems and autonomous driving: advantages and challenges. IEEE Signal Processing Magazine, 2020, 37(4): 98–117.

[7] JOHANSSON T, ORBOM A, SUME A, et al. Radar measurements of moving objects around corners in a realistic scene. Proc. of the Conference on Radar Sensor Technology XVIII, 2014. DOI: 10.1117/12.2049588.

[8] SOLOMITCKII D, BARNETO C, TURUNEN M, et al. Millimeter-wave automotive radar scheme with passive reflector for blind corner conditions. Proc. of the 14th European Conference on Antennas and Propagation, 2020. DOI: 10.23919/EuCAP48036.2020.9135926.

[9] SOLOMITCKII D, BARNETO C, TURUNEN M, et al. Millimeter-wave radar scheme with passive reflector for uncontrolled blind urban intersection. IEEE Trans. on Vehicular Technology, 2021, 70(8): 7335–7346.

[10] SOLOMITCKII D, HEINO M, BUDDAPPAGARI S, et al. Radar scheme with raised reflector for NLOS vehicle detection. IEEE Trans. on Intelligent Transportation Systems, 2021, 23(7): 9037–9045.

[11] ZHANG Z Z, KO S W, WANG R, et al. Multi-point vehicular positioning via millimeter-wave transmissions. Proc. of the 34th International Technical Conference on Circuits/Systems, Computers and Communications, 2019. DOI:10.1109/ITC-CSCC.2019.8793362.

[12] ZHANG Z Z, KO S W, WANG R, et al. Millimeter-wave multipoint vehicular positioning for autonomous driving. Proc. of the IEEE Global Communications Conference, 2019. DOI: 10.1109/GLOBECOM38437.2019.9013613.

[13] ZHANG Z Z, KO S W, WANG R, et al. Cooperative multipoint vehicular positioning using millimeter-wave surface reflection. IEEE Trans. on Wireless Communications, 2021, 20(4): 2221–2236.

[14] ALADSANI M, ALKHATEEB A, TRICHOPOULOS G. Leveraging MMwave imaging and communications for simultaneous localization and mapping. Proc. of the IEEE International Conference on Acoustics, Speech and Signal Processing, 2019: 4539–4543.

[15] SCHEINER N, KRAUS F, WEI F Y, et al. Seeing around street corners: non-line-of-sight detection and tracking in-the-wild using Doppler radar. Computer Vision and Pattern Recognition, 2020. DOI: 10.48550/arXiv.1912.06613.

[16] CORVAJA R, ARMADA A. Analysis of SVD-based hybrid schemes for massive MIMO with phase noise and imperfect channel estimation. IEEE Trans. on Vehicular Technology, 2020, 69(7): 7325–7338.

[17] PREVOST C, USEVICH K, COMON P, et al. Hyperspectral super resolution with coupled tucker approximation: recoverability and SVD based algorithms. IEEE Trans. on Signal Processing, 2020, 68: 931–946.

[18] MENG H, WANG K, GAO Y, et al. Adaptive Gaussian weighted lap lace prior regularization enables accurate morphological reconstruction in fluorescence molecular tomography. IEEE Trans. on Medical Imaging, 2019, 38(12): 2726–2734.

[19] YASIN Y, MEHMET A, ALFRED O H. Multimodal data fusion in high-dimensional heterogeneous datasets via generative models. IEEE Trans. on Signal Processing, 2021, 69:

5175–5188.
[20] GUO Y F, LIAO G S, LI J, et al. A novel moving target detection method based on RPCA for SAR systems. IEEE Trans. on Geoscience and Remote Sensing, 2020, 58(9): 6677–6690.
[21] UZAIR M, BRINKWORTH R S, FINN A. Bio-inspired video enhancement for small moving target detection. IEEE Trans. on Image Processing, 2021, 30: 1232–1244.
[22] VITO A, MORRETI G. Probability of false alarm in CA-CFAR device downstream from linear-law detector. Electronics Letters, 1990, 25(25): 1692–1693.
[23] LU S P, DING F, LI R W. Robust centralized CFAR detection for multistatic sonar systems. Chinese Journal of Electronics, 2021, 30(2): 322–330.
[24] GUO S S, ZHAO Q S, CUI G L, et al. Behind corner targets location using small aperture millimeter wave radar in NLOS urban environment. IEEE Journal of Selected Topics in Applied Earth Observations and Remote Sensing, 2020, 13: 460–470.
[25] LI S L, GUO S S, CHEN J H, et al. Multiple targets localization behind L-shaped corner via UWB radar. IEEE Trans. on Vehicular Technology, 2021, 70(4): 3087–3100.
[26] LI H Q, CUI G L, KONG L J, et al. Scale-adaptive human target tracking for through-wall imaging radar. IEEE Trans. on Geoscience and Remote Sensing, 2020, 17(8): 1348–1352.
[27] BOONCHOO T, AO X, LIU Y, et al. Grid-based DBSCAN: indexing and inference. Pattern Recognition, 2019, 90: 271–284.
[28] JIN C H, NA H J, PIAO M H, et al. A novel DBSCAN based defect pattern detection and classification framework for wafer bin map. IEEE Trans. on Semiconductor Manufacturing, 2019, 32(3): 286–292.
[29] SHENG D L, DENG J L, XIANG J W. Automatic smoke detection based on SLIC-DBSCAN enhanced convolutional neural network. IEEE Access, 2021, 9: 63933–63942.
[30] SKIDMORE G, CHAWLA T, BEDROSIAN G. Combining physical optics and method of equivalent currents to create unique near-field propagation and scattering technique for automotive radar applications. Proc. of the IEEE International Conference on Microwaves Communications Antennas and Electronic Systems, 2020. DOI: 10.1109/COMCAS44984.2019.8958220.

Biographies

LIU Zhaoyu was born in 1972. He received his B.S. degree from North China University of Water Resources and Electric Power, Zhengzhou, China. He is currently pursuing his Ph.D. degree with the School of Information and Communication Engineering, University of Electronic Science and Technology of China, Chengdu, China. His research interests include signal analysis and non-line-of-sight target detection.
E-mail: dztx08@163.com

ZHANG Wenli was born in 1988. He received his B.S. degree from Hubei University of Technology, Wuhan, China, in 2012, and M.S. and Ph.D. degrees from Chongqing University, Chongqing, China, in 2015 and 2019, respectively. His research interests include signal analysis and non-line-of-sight target detection.
E-mail: 20151201003@cqu.edu.cn

ZHENG Jingyue was born in 1996. She received her B.S. degree from Northwest University, Xi'an, China, in 2019. She is currently pursuing her M.S. degree with the School of Information and Communication Engineering, University of Electronic Science and Technology of China, Chengdu, China. Her research interests include signal analysis and non-line-of-sight target detection.
E-mail: zhengjingyue_uestc@163.com

GUO Shisheng was born in 1990. He received his B.S. degree in communication engineering from Nanchang Hangkong University, Nanchang, China, in 2013, and Ph.D. degree in signal and information processing from University of Electronic Science and Technology of China (UESTC), Chengdu, China, in 2019. He is currently an associate researcher with the School of Information and Communication Engineering, UESTC. His research interests include through-the-wall radar imaging signal analysis, and non-line-of-sight target detection.
E-mail: ssguo@uestc.edu.cn

CUI Guolong was born in 1982. He received his B.S. degree in electronic information engineering and M.S. and Ph.D. degrees in signal and information processing from the University of Electronic Science and Technology of China (UESTC), Chengdu, China, in 2005, 2008, and 2012, respectively. From January 2011 to April 2011, he was a visiting researcher with the University of Naples Federico II, Naples, Italy. From June 2012 to August 2013, he was a postdoctoral researcher with the Department of Electrical and Computer Engineering, Stevens Institute of Technology, Hoboken, NJ, USA. From September 2013 to July 2018, he was an associate professor with UESTC, where he has been a professor since August 2018. His current research interests include cognitive radar, array signal processing, MIMO radar, and through-the-wall radar.
E-mail: cuiguolong@uestc.edu.cn

KONG Lingjiang was born in 1974. He received his B.S. degree in electronic engineering, and M.S. and Ph.D. degrees in signal and information processing from the University of Electronic Science and Technology of China, Chengdu, China, in 1997, 2000, and 2003, respectively. From September 2009 to March 2010, he was a visiting researcher with the University of Florida. He is currently a professor with the School of Information and Communication Engineering, University of Electronic Science and Technology of China. His research interests include multiple-input multiple-output radar, through the-wall radar, and statistical signal processing.
E-mail: lingjiang.kong@gmail.com

LIANG Kun was born in 1988. He received his B.S. degree from North China University of Water Resources and Electric Power, Zhengzhou, in 2012, and Ph.D. degree from Harbin Engineering University, Harbin, China, in 2019, respectively. His research interests include signal analysis and non-line-of-sight target detection.
E-mail: drliangkun@126.com